Acta Cryst E CRYSTALLOGRAPHIC COMMUNICATIONS

ISSN 2056-9890

Synthesis and crystal structure of $Ta_4N_{20}\cdot xN_2$ at megabar pressure

Xuejing He,[a,b,c] James Spender,[c] Qian Zhang,[c] Akun Liang[b]* and Dominique Laniel[c]*

[a]Eastern Institute for Advanced Study, Eastern Institute of Technology, Ningbo, Zhejiang 315200, People's Republic of China, [b]School of Physics, College of Science, Eastern Institute of Technology, Ningbo, Zhejiang 315200, People's Republic of China, and [c]Centre for Science at Extreme Conditions, The University of Edinburgh, Edinburgh EH9 3FD, United Kingdom. *Correspondence e-mail: akliang@eitech.edu.cn, ;dominique.laniel@ed.ac.uk

Received 24 July 2026
Accepted 2 November 2026

This article is part of the collection Early Career Scientists in Structural Science.

Keywords: metal–inorganic framework; tantalum; nitride; high pressure; single-crystal X-ray diffraction.

CCDC reference: 2599864

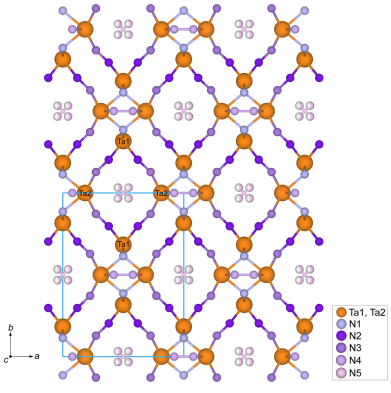
Supporting information: this article has supporting information at journals.iucr.org/e

The title compound $Ta_4N_{20}\cdot xN_2$ (tetratantalum icosanitride dinitrogen), has been synthesized *via* a direct reaction between tantalum carbide (TaC) and molecular nitrogen (N_2) in a laser-heated diamond anvil cell (DAC) at 106 (2) GPa and temperatures above 2600 (200) K. The crystal structure of $Ta_4N_{20}\cdot xN_2$ was determined by *in situ* synchrotron single-crystal X-ray diffraction performed on a polycrystalline sample confined in a DAC at 106 (2) GPa and ambient temperature. The $Ta_4N_{20}\cdot xN_2$ compound crystallizes in the *Cmmm* space group, with an asymmetric unit comprising two Ta crystallographic sites and five N crystallographic sites. The structure contains four distinct nitrogen species: a lone N^{3-} anion, a dinitrogen anion, an armchair-type polymeric nitrogen anion, and a neutral dinitrogen molecule. The tantalum cations are coordinated by the nitrogen species, together forming a three-dimensional metal–inorganic framework, within which the neutral dinitrogen molecules are trapped inside channels extending along the *c*-axis direction. The structure contains at least one N_2 molecule per formula unit; however, the precise value could not be unambiguously determined because of the weak scattering power of nitrogen and likely static disorder of the molecules within the channels. $Ta_4N_{20}\cdot xN_2$ is isostructural to $Hf_4N_{20}\cdot xN_2$ – a here-amended model for the previously reported $Hf_4N_{20}\cdot N_2$ compound [Bykov *et al.* (2020). *Angew. Chem. Int. Ed.* pp. 10321–10326] – and it represents the most nitrogen-rich tantalum nitride reported up to date.

1. Chemical context

Nitrogen, like carbon, is capable of forming single, double, and triple bonds to build a rich variety of structural motifs, allowing for a wide range of molecular and polymeric nitrogen species with distinct structural configurations. However, the high stability of the N≡N triple bond (mean bond enthalpy: 946 kJ mol^{-1}) (Atkins & de Paula, 2006) makes it exceedingly difficult to break, and thus hinders the formation of N—N single (mean bond enthalpy: 163 kJ mol^{-1}) and N=N double (mean bond enthalpy: 409 kJ mol^{-1}) bonds (Atkins & de Paula, 2006); rendering the synthesis of polymeric nitrogen species particularly challenging. The thermodynamic parameter pressure is a powerful means to overcome this challenge by reshaping the Gibbs free energy landscape (Grochala *et al.*, 2007), and has enabled the successful formation of a wide variety of polymeric nitrogen species (*e.g.*, Bykov *et al.*, 2018*a*, 2021; Eremets *et al.*, 2004; Ji *et al.*, 2020; Laniel *et al.*, 2019*a*,*b*, 2020, 2023; Liang *et al.*, 2025).

In particular, the high-pressure synthesis of transition-metal nitrides has attracted considerable attention, as these materials can exhibit remarkable mechanical, electric, and chemical



OPEN ACCESS
Published under a CC BY 4.0 licence

properties under extreme conditions (*e.g.*, Bykov *et al.*, 2019; Aslandukov *et al.*, 2024; Liang *et al.*, 2024). Among transition metal–nitrogen systems, the tantalum–nitrogen (Ta–N) system is particularly attractive as a target for high-pressure studies, given its demonstrated ability to form a wide array of compositionally diverse nitrides. The reported high-pressure phases include the U_2S_3-type Ta_2N_3 (Zerr *et al.*, 2009), the U_3Se_5-type and U_3Te_5-type Ta_3N_5 (Salamat *et al.*, 2014), TaN_{2-x}, TaN_4, and TaN_5 (Bykov *et al.*, 2021).

In this study, we report the synthesis of a new nitrogen-rich tantalum polynitride, $Ta_4N_{20}{\cdot}xN_2$, whose nitrogen content exceeds that of the previously known most nitrogen-rich tantalum nitride, TaN_5 (Bykov *et al.*, 2021). The crystal structure of $Ta_4N_{20}{\cdot}xN_2$ contains four distinct nitrogen species and is isostructural to $Hf_4N_{20}{\cdot}xN_2$ – the latter being a here amended model of the previously reported $Hf_4N_{20}{\cdot}N_2$ compound (Bykov *et al.*, 2020).

2. Structural commentary

$Ta_4N_{20}{\cdot}xN_2$ was synthesized at 106 (2) GPa and crystallizes in the *Cmmm* space group (No. 65), with unit-cell parameters a = 8.5548 (14) Å, b = 11.575 (3) Å, c = 3.548 (2) Å, and V = 351.4 (2) Å^3. Two crystallographically distinct Ta sites are present: Ta1 on the Wyckoff position 4*i* (site symmetry *m*2*m*) and Ta2 on the Wyckoff position 4*h* (site symmetry 2*mm*). The N atoms occupy five crystallographic sites: N1, N4, and N5 are on the Wyckoff positions 4*j* (site symmetry *m*2*m*), 4*g* (site symmetry 2*mm*), and 8*p* (site symmetry ··*m*), respectively, whereas N2 and N3 reside on the general position 16*r*.

In the crystal structure resulting from these atoms (Fig. 1*a*), Ta1 is coordinated to six N atoms, namely two N1 atoms and four N2 atoms, forming a trigonal-prismatic coordination environment (Fig. 1*b*). Ta2 is in a bicapped trigonal-prismatic coordination environment, where two N1 atoms and four N3 atoms define the trigonal prism, and two N4 atoms cap the rectangular faces (Fig. 1*b*). Both the Ta1 and Ta2 trigonal prisms are distorted, leading to a reduction of symmetry from the ideal D_{3h} to C_{2v} (Cremades *et al.*, 2010). As for the N atoms in $Ta_4N_{20}{\cdot}xN_2$, they produce four distinct chemical species (Fig. 1*c*–*f*). The N1 atom, not bonded to any other N atom, can therefore be described as an N^{3-} anion. It is coordinated to both Ta1 and Ta2 (Fig. 1*a*,*b*). The N2 and N3 atoms are arranged in an infinite, fully planar, armchair-type nitrogen chain, $[–N2–N2–N3–N3–]_\infty$ (hereafter written as $[N_4]_\infty$), extending along the *c*-axis direction and contained within or parallel to crystallographic planes approximately described by (570) and ($\bar{5}$70) (Fig. 1*c*,*d*). The N—N bond lengths within the chain, namely d(N2—N2) = 1.24 (11) Å, d(N2—N3) = 1.36 (4) Å, and d(N3—N3) = 1.23 (9) Å at 106 (2) GPa, fall within the typical range for polymeric nitrogen bonds (*e.g.*, Eremets *et al.*, 2004; Bykov *et al.*, 2018*a*,*b*, 2020, 2021). N4 forms an N4—N4 dimer with a bond length of 1.35 (5) Å (Fig. 1*e*). This distance is intermediate between typical N—N single and double bonds, suggesting this dimer to have a charge between 2– and 4– (Laniel *et al.*, 2022). These $(N4)_2$ anions are oriented parallel to the *a* axis, with their centres of mass forming a *C*-centred arrangement. Along with the N1 atoms and the $[N_4]_\infty$ chains, the $(N4)_2$ anions coordinate both Ta1 and Ta2 atoms, thereby forming a three-dimensional framework. Viewed along the *c*-axis direction, this framework exhibits one-dimensional channels with a maximum diameter of 7.343 (3) Å (Fig. 1*a*). The above-described framework (excluding the N2 molecules in the channels; described later) is identical to that previously reported in $Hf_4N_{20}{\cdot}N_2$ at 105 GPa (Bykov *et al.*, 2020).

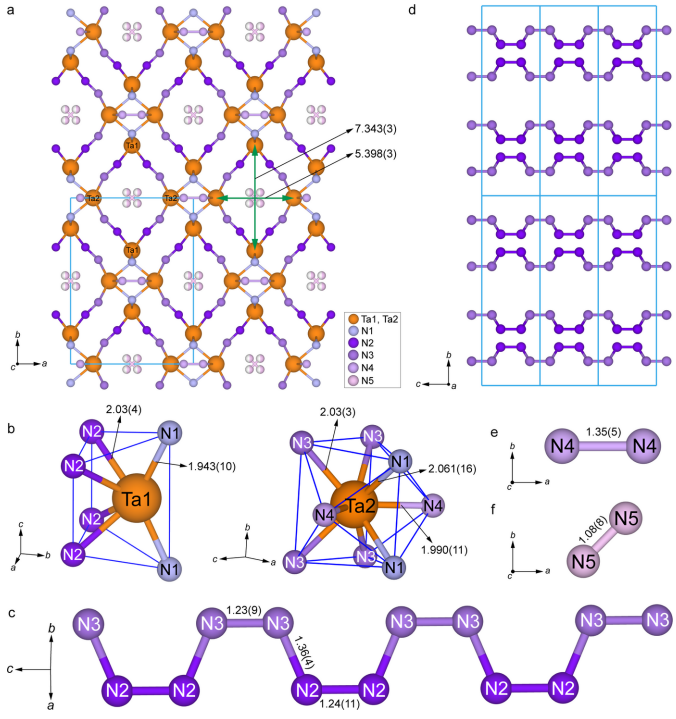


Figure 1
The crystal structure of $Ta_4N_{20}{\cdot}xN_2$ at 106 (2) GPa. (*a*) Projection of the crystal structure along the *c* axis. (*b*) The distorted trigonal-prismatic coordination environment of Ta1 (left) and the distorted bicapped-trigonal-prismatic coordination environment of Ta2 (right). The infinite armchair-type polymeric nitrogen chain (*c*) and its periodic distribution across multiple unit cells, viewed along the *a* axis (*d*) (*f*) The $(N4)_2$ dimer. (*f*) A representative neutral $(N5)_2$ molecule. The light-blue rectangles represent unit cells. All bond lengths and interatomic distances are given in angstroms (Å).

It can be noted that the N2 and N3 atoms constituting the $[N_4]_\infty$ chain show large isotropic displacement parameters (*i.e.*, 0.055 (8) and 0.040 (5) Å^2, respectively) compared with the other N atoms in the structure, having values from 0.011 (4) to 0.019 (8) Å^2. Refinement of their occupancies gave values close to unity [1.10 (14) and 0.92 (6) for N2 and N3, respectively], indicating the $[N_4]_\infty$ chain to have full occupancy. Anisotropic refinement of the displacement parameters of N2 and N3 was also tested, resulting in non-positive-definite displacement parameters for the present dataset. However, in two further $Ta_4N_{20}{\cdot}xN_2$ domains from the same sample, anisotropic refinement was possible for N2 and/or N3, and revealed displacement ellipsoids very elongated perpendicular to the Ta—N bond, *i.e.*, perpendicular to the plane containing the chain. In this direction, the only neighbouring atoms belong to parallel chains [shortest interchain N2···N3

distance: 2.42 (4) Å], which presumably interact only through non-bonding, mainly electrostatic, interactions that are much weaker than the Ta—N bonds. The chain atoms are therefore less constrained in this direction. As N2 and N3 are covalently bonded within the framework and subjected to megabar pressure, the elongated displacements are unlikely to reflect large-amplitude dynamic disorder and more likely arise from static positional disorder of the chains. To test this interpretation, a model with split chain atoms was produced and refined, with the sum of the relevant atomic occupancies fixed to unity. While one of the three $Ta_4N_{20}{\cdot}xN_2$ domains yielded a reasonable split model, seemingly supporting static disorder, its *R* factors are significantly higher than those of the original model, *i.e.*, the model presented in the manuscript, in which no disorder was included and all N atoms were refined isotropically. Indeed, the original model gives $R1 = 0.058$, $wR2 = 0.158$, and GooF = 1.064, whereas the split model gives $R1 = 0.072$, $wR2 = 0.209$, and GooF = 1.095. A more detailed description of this disorder would require future data of higher resolution and completeness.

Within the channels of $Ta_4N_{20}{\cdot}xN_2$, positive residual electron density maxima (*Q* peaks) are observed at two locations along the *c* axis, with values of 4.88 and 4.48 e Å^{-3} (Fig. 2*a*–*c*). By analogy with the N_2 molecules accommodated within the channels of $Hf_4N_{20}{\cdot}N_2$, $WN_8{\cdot}N_2$, $ReN_8{\cdot}xN_2$, and $Os_5N_{28}{\cdot}3N_2$ (Bykov *et al.*, 2018*b*, 2020), these maxima are tentatively assigned to N atoms. The larger maximum (4.88 e Å^{-3}) was first modelled as an N atom with freely refined site occupancy. However, this yielded physically unrealistic results: (1) the site occupancy refined to 1.5; (2) the N—N bond length showed an unreasonably large uncertainty of 1.1 (8) Å; (3) the atomic displacement parameter U_{iso} refined to an abnormally large value of 0.24 (9) Å^2; indicating that this model is untenable despite reasonable *R* factors and GooF ($R1 = 0.058$, $wR2 = 0.165$, GooF = 1.049). However, this seemingly incorrect model is identical to that originally proposed for $Hf_4N_{20}{\cdot}N_2$ (Bykov *et al.*, 2020). On account of this contradiction, we also re-refined the crystallographic data of $Hf_4N_{20}{\cdot}N_2$ (Bykov *et al.*, 2020). When the original CIF (CCDC reference number 1978268) is imported into *OLEX2* (Dolomanov *et al.*, 2009) and the model re-refined, the channel-occupying N_2 molecule collapses into itself; *i.e.* the two atoms of the N_2 molecule merge into a single lone N atom. We note that the structure of $Hf_4N_{20}{\cdot}N_2$ was originally refined using *JANA2006* (Petříček *et al.*, 2016). While that model was verified to be stable in the latter software, its instability in *OLEX2* is thought to result from differences on how the refinement process is handled in the two software.

The stronger maximum (4.88 e Å^{-3}) was therefore left unassigned, and the second maximum (4.48 e Å^{-3}) was instead assigned to an N atom, designated as N5. This yields the structural model shown in Fig. 1*a*. The resulting N5—N5 distance of 1.08 (8) Å is consistent with a triple bond, indicating that two N5 atoms form a neutral N_2 molecule (Fig. 1*f*). Since the N5 atoms occupy the 8*p* Wyckoff site (site symmetry ··*m*), the crystallographically equivalent sites define two possible orientations of the N_2 molecule (Fig. 1*a*), both sharing the same centre of mass. As only one of the orientations can be occupied at a time, the short N5···N5 distances of 0.76 (8) and 0.77 (8) Å between atoms of different orientations have

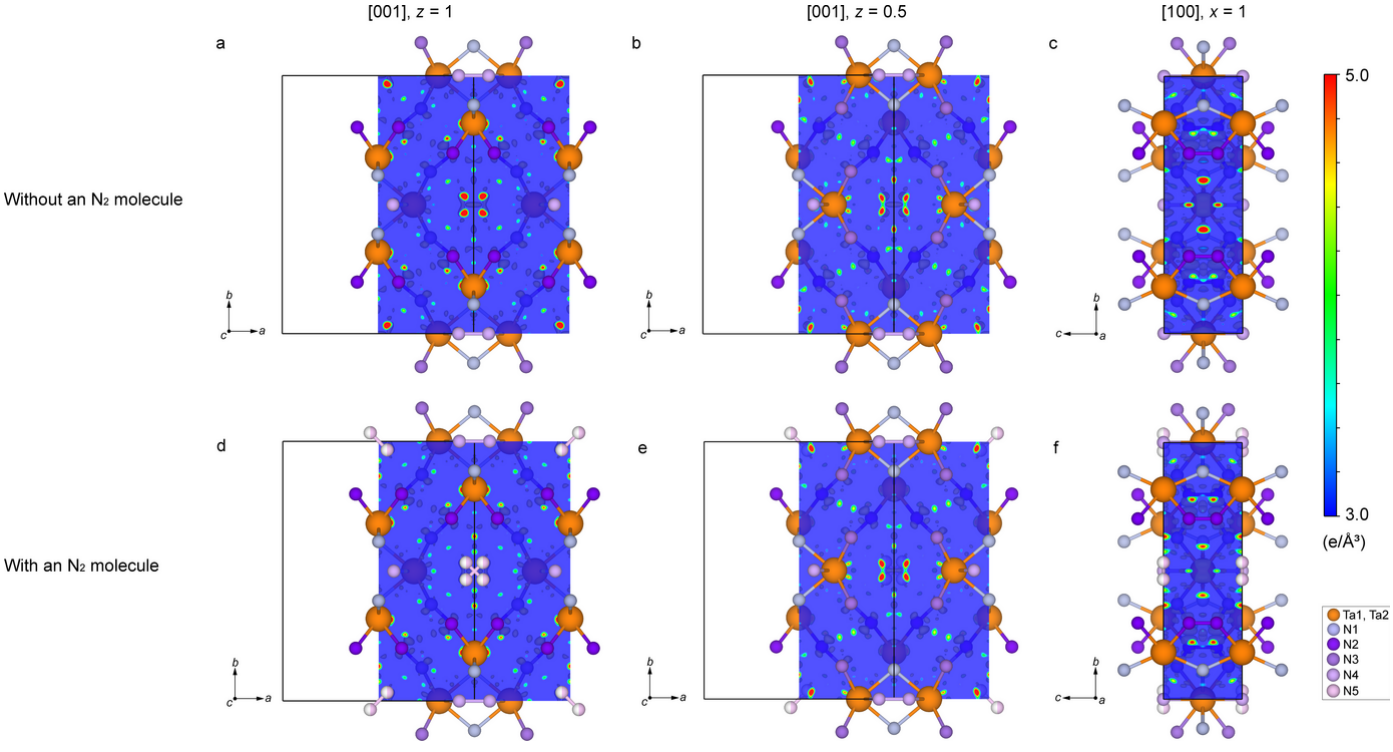


Figure 2
Difference-Fourier maps viewed perpendicular to and parallel to the channel axis of the $Ta_4N_{20}{\cdot}xN_2$ compound at 106 (2) GPa, before (*a*), (*b*), (*c*) and after (*d*), (*e*), (*f*) modeling the residual electron density in the channel with a disordered N_2 molecule.

no physical meaning. Free refinement of site occupancy yielded a value of 0.646, slightly exceeding the physically permissible maximum of 0.5 for this model. This mildly elevated occupancy is attributed to additional unmodeled electron density within the channel, as well as the limited completeness of the dataset. However, unlike the previous model, the N5—N5 bond length and the isotropic displacement parameter [U_{iso} = 0.019 (8) Å^2] remain reasonable. The occupancy was therefore fixed to 0.5, yielding a chemical formula of $Ta_4N_{20}{\cdot}N_2$ ($R1$ = 0.058, $wR2$ = 0.158, GooF = 1.064). Nevertheless, residual Q peaks persist within the channels (Fig. 2*d*–*f*), which suggests some degree of static disorder of the N_2 molecules. This part of the structure is therefore not uniquely determined by the present diffraction data, and the proposed model should be regarded as the best description achievable with the present data quality. Given the likelihood of additional nitrogen species being within the channels, we propose the chemical formula $Ta_4N_{20}{\cdot}xN_2$, in analogy with another metal-inorganic framework, $ReN_8{\cdot}xN_2$ (Bykov *et al.*, 2018*b*).

Applying the model developed in this work to the $Hf_4N_{20}{\cdot}N_2$ dataset (Bykov *et al.*, 2020) yields, in *OLEX2*, satisfactory R factors and GooF ($R1$ = 0.083, $wR2$ = 0.208, GooF = 1.083). However, residual electron density (11.88 e Å^{-3}) persists along the *c*-axis direction within the channels, consistent with our observations in $Ta_4N_{20}{\cdot}xN_2$. The presence of additional nitrogen molecules in the channels may partly account for the discrepancy between the experimental pressure (105 GPa) and that of the DFT-relaxed structure (93–96.4 GPa, depending on the functional used) reported by Bykov *et al.* (2020). A full characterization of the N entities within the channels, outside the scope of this paper, will require high-resolution diffraction studies combined with DFT-based molecular dynamics. It can also be noted that the corresponding N2 and N3 sites in the $Hf_4N_{20}{\cdot}N_2$ dataset also show similarly large isotropic displacement parameters, both in the original refinement [0.045 (6) and 0.025 (4) Å^2, respectively; Bykov *et al.*, 2020] and in our re-refinement [0.046 (7) and 0.030 (4) Å^2, respectively], further supporting the above interpretation of static disorder in the $[N_4]_\infty$ chain.

A tentative charge-balance analysis, based on the refined N—N bond lengths, was also performed for the $Ta_4N_{20}{\cdot}xN_2$ compound. Based on its asymmetric unit it is comprised of one Ta1, one Ta2, one N1, four N2, four N3, one N4, and two N5 atoms (but with site occupancy 0.5). Assuming Ta1 and Ta2 to be in their most common oxidation state of +5, assigning N1 as N^{3-}, and considering the $(N5)_2$ molecule to be neutral, charge balance requires $a + b = -7$. Here, a denotes the charge on each N4 atom. Since two N4 atoms form the N4—N4 dimer, the dimer can be written as $[N_2]^{2a}$. Likewise, b denotes the total charge carried by the four N2 and four N3 atoms forming the armchair-type chain, corresponding to $[N_4]_\infty^{b/2}$ per repeat unit. The N4—N4 bond length of 1.35 (5) Å is consistent with a bond order between one and two (Laniel *et al.*, 2022), suggesting a charge between −1 and −2 per N4 atom (*i.e.*, between $[N_2]^{2-}$ and $[N_2]^{4-}$). If $a = -1$, then the four N2 and four N3 atoms must carry a total charge of $b = -6$, corresponding to a chain charge of $[N_4]_\infty^{3-}$. Conversely, if $a = -2$, the chain charge becomes $[N_4]_\infty^{2.5-}$. With the present diffraction data, distinguishing between these two charge configurations is not possible, and the formal charges proposed here remain an interpretation based on bond lengths. In related structures, *i.e.*, $Hf_4N_{20}{\cdot}N_2$, $WN_8{\cdot}N_2$, $ReN_8{\cdot}xN_2$, and $Os_5N_{28}{\cdot}3N_2$ (Bykov *et al.*, 2018*b*, 2020), theoretical calculations have been employed to corroborate the nature of the bonds, helping to mitigate the lower precision in the positions of the N atoms due to the limited opening angle of the DAC and the weak X-ray scattering of N relative to Ta. In $Hf_4N_{20}{\cdot}N_2$, the $[N_4]_\infty$ chain and the $[N_2]$ dimer were both assigned a charge of −2, yielding an oxidation state of +4 for Hf, its most common value (Bykov *et al.*, 2020).

Overall, although the structural model used to describe the channel-occupying nitrogen species in $Ta_4N_{20}{\cdot}xN_2$ differs from that originally proposed for $Hf_4N_{20}{\cdot}N_2$ [synthesized at 105 GPa, 1900 (200) K; Bykov *et al.*, 2020], our analysis demonstrates that the electron-density distribution within the channels is consistent between the two structures, and we therefore conclude that the two compounds are isostructural, with $Hf_4N_{20}{\cdot}N_2$ actually being $Hf_4N_{20}{\cdot}xN_2$. Similar structures are also observed for $WN_8{\cdot}N_2$ [105 GPa, 2700 (200) K], $ReN_8{\cdot}xN_2$ [123 GPa, 2700 (200) K], and $Os_5N_{28}{\cdot}3N_2$ [106 GPa, 2800 (150) K] (Bykov *et al.*, 2018*b*, 2020), all synthesized in adjacent 5*d* transition metal-nitrogen systems under comparable high-pressure and high-temperature conditions. This strongly suggests that this structure type is a recurring feature in 5*d* transition metal nitrides at megabar pressures.

3. Synthesis and crystallization

$Ta_4N_{20}{\cdot}xN_2$ was synthesized under high-pressure and high-temperature conditions using a laser-heated diamond anvil cell (LHDAC). In this study, a BX90-type DAC equipped with a pair of Boehler-Almax type diamond anvils (120 µm culet diameter) was employed. Tantalum carbide (TaC) powder (Goodfellow Advanced Materials, 99.5% purity) was loaded into the sample chamber formed by a rhenium (Re) gasket preindented to a thickness of 18 µm and laser-drilled to obtain a 60 µm diameter hole. Molecular nitrogen (N_2, BOC Gases, research grade, 99.9995% purity), serving both as a reagent and as the pressure transmitting medium, was then loaded into the sample chamber at 2000 bar using a home-built gas-loading system. Pressure in the sample chamber was determined from the diamond anvil based on the pressure-induced shift of its Raman band (Akahama & Kawamura, 2006) and from the Re gasket edge using its measured unit cell parameters, accordingly to the equation of state reported by Anzellini *et al.* (2014). Upon compression to 106 (2) GPa, TaC and N_2 were laser-heated from both sides of the DAC using a home-built laser-heating system with an ytterbium fiber laser (λ = 1070 nm). While the maximum measured temperature was 2600 (200) K, determined based on the measured sample's thermal emission fitted to Planck's law, even higher temperatures are thought to have been reached based on the

Table 1
Experimental details.

Crystal data	
Chemical formula	$Ta_4N_{20}{\cdot}N_2$
M_r	1032.02
Crystal system, space group	Orthorhombic, *Cmmm*
Temperature (K)	293
Pressure (kPa)	1.06 (2) × 10^8
a, *b*, *c* (Å)	8.5548 (14), 11.575 (3), 3.548 (2)
V (Å^3)	351.4 (2)
Z	2
Radiation type	Synchrotron, λ = 0.2846 Å
μ (mm^{-1})	5.70
Crystal size (mm)	0.001 × 0.001 × 0.001
Data collection	
Diffractometer	Customized ω-circle diffractometer at ID11, ESRF (Wright *et al.*, 2020)
Absorption correction	Multi-scan (*CrysAlis PRO*; Rigaku OD, 2025)
T_{min}, T_{max}	0.151, 1.000
No. of measured, independent and observed [$I > 2\sigma(I)$] reflections	993, 407, 284
R_{int}	0.074
(sin $\theta/\lambda)_{max}$ (Å^{-1})	0.942
Refinement	
$R[F^2 > 2\sigma(F^2)]$, $wR(F^2)$, *S*	0.058, 0.158, 1.06
No. of reflections	407
No. of parameters	24
$\Delta\rho_{max}$, $\Delta\rho_{min}$ (e Å^{-3})	4.84, −5.47

Computer programs: beamline control software at ID11, ESRF (Wright *et al.*, 2020), *CrysAlis PRO* (Rigaku OD, 2025), *SHELXT2018/2* (Sheldrick, 2015*a*), *SHELXL2014/7* (Sheldrick, 2015*b*), *OLEX2* 1.5 (Dolomanov *et al.*, 2009) and *VESTA* (Momma & Izumi, 2011).

visual observation of the thermal emission. The resulting chemical reaction produced a multiphase product consisting of agglomerates of numerous submicrometer-sized crystallites, with $Ta_4N_{20}{\cdot}xN_2$ present as one of the constituents. $Ta_4N_{20}{\cdot}xN_2$ was detected only at the synthesis pressure of 106 (2) GPa; upon sample decompression, the phase was no longer observed at 94 (2) GPa, indicating that it is not recoverable under ambient conditions.

4. Refinement

Crystal data, data collection and structure refinement details are summarized in Table 1. The crystal structure of $Ta_4N_{20}{\cdot}xN_2$ was determined by *in-situ* high-pressure multi-grain single-crystal XRD (SCXRD) using synchrotron radiation. X-ray diffraction experiments were conducted at the ID11 beamline of the European Synchrotron Radiation Facility's Extreme Brilliant Source (ESRF-EBS) (Wright *et al.*, 2020). The monochromatic X-ray wavelength was 0.2846 Å, and the beam size was focused to 1 µm×1 µm. Diffraction data were collected with an Eiger2X CdTe 4M hybrid photon counting pixel detector. To locate suitable spots for SCXRD measurements, a 2D XRD mapping of the laser-heated region was performed with a step size of 1 µm, with the DAC at $\omega = 0°$ and one diffraction pattern collected at each position. From the resulting map, built and analyzed using the *XDI* software and the *Dioptas* software (Hrubiak *et al.*, 2019; Prescher & Prakapenka, 2015), SCXRD data were collected on selected spots exhibiting the most intense single-crystal reflections belonging to the phase of interest. During data collection, the DAC was rotated about its vertical axis from $\omega = -36°$ to +36° in 0.5° increments.

The SCXRD data were processed using the *CrysAlis PRO* software package (version 45.67; Rigaku OD, 2025), including peak hunting, indexing, integration, frame scaling, absorption correction, and preparation of files for subsequent structure refinement. The instrument model in *CrysAlis PRO* was calibrated using diffraction data from an orthoenstatite crystal $[(Mg_{1.93}Fe_{0.06})(Si_{1.93}Al_{0.06})O_6$, *Pbca*, *a* = 8.8117 (2) Å, *b* = 5.18320 (10) Å, *c* = 18.2391 (3) Å], including refinement of the sample-to-detector distance, detector origin, detector tilt, beam direction, and goniometer angle offsets. The *DAFi* program integrated within *CrysAlis PRO* was used to identify groups of reflections belonging to individual single-crystal domains within the multigrain SCXRD dataset, enabling their separation prior to subsequent indexing (Aslandukov *et al.*, 2022). Structures were solved using the *SHELXT* program (Sheldrick, 2015*a*) by intrinsic phasing and subsequently refined by least-squares minimization using *SHELXL* (Sheldrick, 2015*b*) within the *OLEX2* software package (Dolomanov *et al.*, 2009). Crystal structures were visualized using the *VESTA* software (Momma & Izumi, 2011).

Acknowledgements

The authors acknowledge the European Synchrotron Radiation Facility for provision of beamtime under proposal number HC-5808, and we would like to thank Dr Jonathan Wright for assistance in using beamline ID11. The authors are grateful to Sarah Bolton (The University of Edinburgh), Dr Hannah Shuttleworth (The University of Edinburgh), Dr Keishiro Yamashita (The University of Edinburgh), and Dr Andrey Aslandukov (Goethe Frankfurt University) for discussions.

Funding information

AL acknowledges the National Natural Science Foundation of China (NSFC) (grant No. 12504015) for financial support. DL acknowledges the UKRI Future Leaders Fellowship (grant No. MR/V025724/1) for financial support.

References

Akahama, Y. & Kawamura, H. (2006). *J. Appl. Phys.* **100**, 043516.
Anzellini, S., Dewaele, A., Occelli, F., Loubeyre, P. & Mezouar, M. (2014). *J. Appl. Phys.* **115**, 043511.
Aslandukov, A., Aslandukov, M., Dubrovinskaia, N. & Dubrovinsky, L. (2022). *J. Appl. Cryst.* **55**, 1383–1391.
Aslandukov, A., Liang, A., Ehn, A., Trybel, F., Yin, Y., Aslandukova, A., Akbar, F. I., Ranieri, U., Spender, J., Howie, R. T., Bright, E. L., Wright, J., Hanfland, M., Garbarino, G., Mezouar, M., Fedotenko, T., Abrikosov, I. A., Dubrovinskaia, N., Dubrovinsky, L. & Laniel, D. (2024). *J. Am. Chem. Soc.* **146**, 18161–18171.

Atkins, P. & de Paula, J. (2006). *Atkins' Physical Chemistry* 8th ed., p. 1012. New York: W. H. Freeman.

Bykov, M., Bykova, E., Aprilis, G., Glazyrin, K., Koemets, E., Chuvashova, I., Kupenko, I., McCammon, C., Mezouar, M., Prakapenka, V., Liermann, H.-P., Tasnádi, F., Ponomareva, A. V., Abrikosov, I. A., Dubrovinskaia, N. & Dubrovinsky, L. (2018*a*). *Nat. Commun.* **9**, 2756.

Bykov, M., Bykova, E., Koemets, E., Fedotenko, T., Aprilis, G., Glazyrin, K., Liermann, H.-P., Ponomareva, A. V., Tidholm, J., Tasnádi, F., Abrikosov, I. A., Dubrovinskaia, N. & Dubrovinsky, L. (2018*b*). *Angew. Chem. Int. Ed.* **57**, 9048–9053.

Bykov, M., Bykova, E., Ponomareva, A. V., Abrikosov, I. A., Chariton, S., Prakapenka, V. B., Mahmood, M. F., Dubrovinsky, L. & Goncharov, A. F. (2021). *Angew. Chem. Int. Ed.* **60**, 9003–9008.

Bykov, M., Chariton, S., Bykova, E., Khandarkhaeva, S., Fedotenko, T., Ponomareva, A. V., Tidholm, J., Tasnádi, F., Abrikosov, I. A., Sedmak, P., Prakapenka, V., Hanfland, M., Liermann, H.-P., Mahmood, M., Goncharov, A. F., Dubrovinskaia, N. & Dubrovinsky, L. (2020). *Angew. Chem. Int. Ed.* **59**, 10321–10326.

Bykov, M., Chariton, S., Fei, H., Fedotenko, T., Aprilis, G., Ponomareva, A. V., Tasnádi, F., Abrikosov, I. A., Merle, B., Feldner, P., Vogel, S., Schnick, W., Prakapenka, V. B., Greenberg, E., Hanfland, M., Pakhomova, A., Liermann, H.-P., Katsura, T., Dubrovinskaia, N. & Dubrovinsky, L. (2019). *Nat. Commun.* **10**, 2994.

Cremades, E., Echeverría, J. & Alvarez, S. (2010). *Chem. A Eur. J.* **16**, 10380–10396.

Dolomanov, O. V., Bourhis, L. J., Gildea, R. J., Howard, J. A. K. & Puschmann, H. (2009). *J. Appl. Cryst.* **42**, 339–341.

Eremets, M. I., Gavriliuk, A. G., Trojan, I. A., Dzivenko, D. A. & Boehler, R. (2004). *Nat. Mater.* **3**, 558–563.

Grochala, W., Hoffmann, R., Feng, J. & Ashcroft, N. W. (2007). *Angew. Chem. Int. Ed.* **46**, 3620–3642.

Hrubiak, R., Smith, J. S. & Shen, G. (2019). *Rev. Sci. Instrum.* **90**, 025109.

Ji, C., Adeleke, A. A., Yang, L., Wan, B., Gou, H., Yao, Y., Li, B., Meng, Y., Smith, J. S., Prakapenka, V. B., Liu, W., Shen, G., Mao, W. L. & Mao, H.-K. (2020). *Sci. Adv.* **6**, eaba9206.

Laniel, D., Geneste, G., Weck, G., Mezouar, M. & Loubeyre, P. (2019*a*). *Phys. Rev. Lett.* **122**, 066001.

Laniel, D., Trybel, F., Yin, Y., Fedotenko, T., Khandarkhaeva, S., Aslandukov, A., Aprilis, G., Abrikosov, A. I., Masood, T. B., Giacobbe, C., Bright, E. L., Glazyrin, K., Hanfland, M., Wright, J., Hotz, I., Abrikosov, I. A., Dubrovinsky, L. & Dubrovinskaia, N. (2023). *Nat. Chem.* **15**, 641–646.

Laniel, D., Winkler, B., Fedotenko, T., Aslandukova, A., Aslandukov, A., Vogel, S., Meier, T., Bykov, M., Chariton, S., Glazyrin, K., Milman, V., Prakapenka, V., Schnick, W., Dubrovinsky, L. & Dubrovinskaia, N. (2022). *Phys. Rev. Mater.* **6**, 023402.

Laniel, D., Winkler, B., Fedotenko, T., Pakhomova, A., Chariton, S., Milman, V., Prakapenka, V., Dubrovinsky, L. & Dubrovinskaia, N. (2020). *Phys. Rev. Lett.* **124**, 216001.

Laniel, D., Winkler, B., Koemets, E., Fedotenko, T., Bykov, M., Bykova, E., Dubrovinsky, L. & Dubrovinskaia, N. (2019*b*). *Nat. Commun.* **10**, 4515.

Liang, A., Osmond, I., Krach, G., Shi, L.-T., Brüning, L., Ranieri, U., Spender, J., Tasnadi, F., Massani, B., Stevens, C. R., McWilliams, R. S., Bright, E. L., Giordano, N., Gallego–Parra, S., Yin, Y., Aslandukov, A., Akbar, F. I., Gregoryanz, E., Huxley, A., Peña–Alvarez, M., Si, J.-G., Schnick, W., Bykov, M., Trybel, F. & Laniel, D. (2024). *Adv. Funct. Mater.* **34**, 2313819.

Liang, A., ten Eikelder, H. R. A., Ranieri, U., Spender, J., Massani, B., Fedotenko, T., Glazyrin, K., Giordano, N., Bright, E. L., Wright, J., Shi, L.-T., Trybel, F. & Laniel, D. (2025). *JACS Au* **6**, 193–199.

Momma, K. & Izumi, F. (2011). *J. Appl. Cryst.* **44**, 1272–1276.

Petříček, V., Dušek, M. & Plášil, J. (2016). *Z. Kristallogr.* **231**, 583–599.

Prescher, C. & Prakapenka, V. B. (2015). *High Pressure Res.* **35**, 223–230.

Rigaku OD (2025). *CrysAlis PRO*. Rigaku Oxford Diffraction Ltd, Yarnton, England.

Salamat, A., Woodhead, K., Shah, S. I. U., Hector, A. L. & McMillan, P. F. (2014). *Chem. Commun.* **50**, 10041–10044.

Sheldrick, G. M. (2015*a*). *Acta Cryst.* A**71**, 3–8.

Sheldrick, G. M. (2015*b*). *Acta Cryst.* C**71**, 3–8.

Wright, J., Giacobbe, C. & Majkut, M. (2020). *Curr. Opin. Solid State Mater. Sci.* **24**, 100818.

Zerr, A., Miehe, G., Li, J., Dzivenko, D. A., Bulatov, V. K., Höfer, H., Bolfan–Casanova, N., Fialin, M., Brey, G., Watanabe, T. & Yoshimura, M. (2009). *Adv. Funct. Mater.* **19**, 2282–2288.

supporting information

Acta Cryst. (2026). E**82** [https://doi.org/10.1107/S2056989026011394]

Synthesis and crystal structure of $Ta_4N_{20}{\cdot}xN_2$ at megabar pressure

Xuejing He, James Spender, Qian Zhang, Akun Liang and Dominique Laniel

Computing details

Tetratantalum icosanitride dinitrogen

Crystal data

$Ta_4N_{20}{\cdot}N_2$
M_r = 1032.02
Orthorhombic, *Cmmm*
a = 8.5548 (14) Å
b = 11.575 (3) Å
c = 3.548 (2) Å
V = 351.4 (2) Å^3
Z = 2
F(000) = 892
D_x = 9.755 Mg m^{-3}
Synchrotron radiation, λ = 0.2846 Å
Cell parameters from 274 reflections
θ = 1.9–16.4°
μ = 5.70 mm^{-1}
T = 293 K
Block, black
0.001 × 0.001 × 0.001 mm

Data collection

Customized ω-circle diffractometer at ID11, ESRF (Wright *et al.*, 2020)
Radiation source: synchrotron
Synchrotron monochromator
Detector resolution: 13.3333 pixels mm^{-1}
ω scans
Absorption correction: multi-scan (CrysAlisPro; Rigaku OD, 2025)
T_{min} = 0.151, T_{max} = 1.000
993 measured reflections
407 independent reflections
284 reflections with $I > 2\sigma(I)$
R_{int} = 0.074
θ_{max} = 15.6°, θ_{min} = 1.9°
h = −16→16
k = −21→20
l = −4→4

Refinement

Refinement on F^2
Least-squares matrix: full
$R[F^2 > 2\sigma(F^2)]$ = 0.058
$wR(F^2)$ = 0.158
S = 1.06
407 reflections
24 parameters
0 restraints
Primary atom site location: dual
$w = 1/[\sigma^2(F_o^2) + (0.0797P)^2]$ where $P = (F_o^2 + 2F_c^2)/3$
$(\Delta/\sigma)_{max} < 0.001$
$\Delta\rho_{max}$ = 4.84 e Å^{-3}
$\Delta\rho_{min}$ = −5.47 e Å^{-3}

Special details

Experimental. High-pressure measurement at 106 (2) GPa in a BX90-type diamond anvil cell with effective opening angle of 76 deg., and molecular N2 was used as a pressure transmitting medium. Pressure was determined from the anvil's high-frequency Raman signal edge and corroborated with the diffraction signal of the rhenium gasket edge, according to the equation of state of rhenium.

Geometry. All esds (except the esd in the dihedral angle between two l.s. planes) are estimated using the full covariance matrix. The cell esds are taken into account individually in the estimation of esds in distances, angles and torsion angles; correlations between esds in cell parameters are only used when they are defined by crystal symmetry. An approximate (isotropic) treatment of cell esds is used for estimating esds involving l.s. planes.

Fractional atomic coordinates and isotropic or equivalent isotropic displacement parameters (Å²)

	x	*y*	*z*	U_{iso}*/U_{eq}	Occ. (<1)
Ta1	0.0000	0.18280 (9)	0.0000	0.0078 (4)	
Ta2	0.18453 (13)	0.0000	0.5000	0.0110 (4)	
N1	0.0000	0.114 (2)	0.5000	0.011 (4)*	
N2	0.120 (2)	0.297 (3)	0.325 (16)	0.055 (8)*	
N3	0.226 (2)	0.372 (2)	0.174 (13)	0.040 (5)*	
N4	0.079 (3)	0.0000	0.0000	0.011 (4)*	
N5	0.044 (5)	0.467 (4)	0.0000	0.019 (8)*	0.5

Atomic displacement parameters (Å²)

	U^{11}	U^{22}	U^{33}	U^{12}	U^{13}	U^{23}
Ta1	0.0107 (4)	0.0068 (5)	0.0059 (12)	0.000	0.000	0.000
Ta2	0.0085 (4)	0.0145 (6)	0.0098 (14)	0.000	0.000	0.000

Geometric parameters (Å, º)

Ta1—N1^{i}	1.943 (10)	Ta2—N3^{xii}	2.03 (3)
Ta1—N1	1.943 (10)	Ta2—N3^{vi}	2.03 (3)
Ta1—N2^{ii}	2.03 (4)	Ta2—N3^{xiii}	2.03 (3)
Ta1—N2^{iii}	2.03 (4)	Ta2—N3^{xiv}	2.03 (3)
Ta1—N2	2.03 (4)	Ta2—N4	1.990 (11)
Ta1—N2^{iv}	2.03 (4)	Ta2—N4^{x}	1.990 (11)
Ta1—N3^{v}	2.50 (2)	N1—Ta1^{x}	1.943 (10)
Ta1—N3^{vi}	2.50 (2)	N1—Ta2^{xi}	2.061 (16)
Ta1—N3^{vii}	2.50 (2)	N2—N2^{xv}	1.24 (11)
Ta1—N3^{viii}	2.50 (2)	N2—N3	1.36 (4)
Ta1—N4^{ix}	2.222 (7)	N3—Ta1^{vii}	2.50 (2)
Ta1—N4	2.222 (7)	N3—Ta2^{xiii}	2.03 (3)
Ta2—Ta1^{ix}	3.1807 (11)	N3—N3^{ii}	1.23 (9)
Ta2—Ta1^{x}	3.1807 (11)	N4—Ta1^{ix}	2.222 (7)
Ta2—Ta2^{xi}	3.157 (2)	N4—Ta2^{i}	1.990 (11)
Ta2—N1^{xi}	2.061 (16)	N4—N4^{ix}	1.35 (5)
Ta2—N1	2.061 (16)	N5—N5^{xvi}	1.08 (8)
N1^{i}—Ta1—N1	131.9 (13)	N1—Ta2—N1^{xi}	80.0 (10)
N1^{i}—Ta1—N2^{ii}	75.4 (15)	N3^{xiv}—Ta2—Ta1^{x}	172.2 (6)
N1—Ta1—N2	75.4 (15)	N3^{xii}—Ta2—Ta1^{ix}	91.1 (9)
N1—Ta1—N2^{iii}	141.5 (14)	N3^{xiii}—Ta2—Ta1^{x}	51.9 (7)
N1—Ta1—N2^{iv}	75.4 (15)	N3^{xii}—Ta2—Ta1^{x}	110.8 (11)
N1—Ta1—N2^{ii}	141.5 (13)	N3^{xiv}—Ta2—Ta1^{ix}	51.9 (7)

N1^{i}—Ta1—N2	141.5 (13)	N3^{vi}—Ta2—Ta1	51.9 (7)
N1^{i}—Ta1—N2^{iv}	141.5 (13)	N3^{xiii}—Ta2—Ta1	91.1 (9)
N1^{i}—Ta1—N2^{iii}	75.4 (15)	N3^{xii}—Ta2—Ta1	172.2 (6)
N1—Ta1—N3^{vi}	70.9 (9)	N3^{vi}—Ta2—Ta1^{x}	91.1 (9)
N1—Ta1—N3^{viii}	70.9 (10)	N3^{vi}—Ta2—Ta1^{ix}	110.8 (11)
N1—Ta1—N3^{v}	97.0 (10)	N3^{xiv}—Ta2—Ta1	110.8 (11)
N1—Ta1—N3^{vii}	97.0 (10)	N3^{xiii}—Ta2—Ta1^{ix}	172.2 (6)
N1^{i}—Ta1—N3^{vi}	97.0 (10)	N3^{xii}—Ta2—Ta2^{xi}	112.1 (7)
N1^{i}—Ta1—N3^{viii}	97.0 (10)	N3^{xiv}—Ta2—Ta2^{xi}	112.1 (7)
N1^{i}—Ta1—N3^{vii}	70.9 (10)	N3^{vi}—Ta2—Ta2^{xi}	112.1 (7)
N1^{i}—Ta1—N3^{v}	70.9 (9)	N3^{xiii}—Ta2—Ta2^{xi}	112.1 (7)
N1^{i}—Ta1—N4^{ix}	67.2 (6)	N3^{xii}—Ta2—N1	139.3 (10)
N1—Ta1—N4^{ix}	67.2 (6)	N3^{vi}—Ta2—N1^{xi}	139.3 (10)
N1^{i}—Ta1—N4	67.2 (6)	N3^{xiv}—Ta2—N1	139.3 (10)
N1—Ta1—N4	67.2 (6)	N3^{xiv}—Ta2—N1^{xi}	79.6 (8)
N2^{iii}—Ta1—N2	99 (2)	N3^{xiii}—Ta2—N1^{xi}	139.3 (10)
N2^{ii}—Ta1—N2	69 (3)	N3^{xii}—Ta2—N1^{xi}	79.6 (8)
N2^{iv}—Ta1—N2^{iii}	69 (3)	N3^{vi}—Ta2—N1	79.6 (8)
N2^{iii}—Ta1—N2^{ii}	60.7 (16)	N3^{xiii}—Ta2—N1	79.6 (8)
N2^{iv}—Ta1—N2	60.7 (16)	N3^{vi}—Ta2—N3^{xii}	135.8 (13)
N2^{iv}—Ta1—N2^{ii}	99 (2)	N3^{xiv}—Ta2—N3^{xii}	69 (2)
N2^{ii}—Ta1—N3^{vi}	80.3 (12)	N3^{xiv}—Ta2—N3^{vi}	93.8 (18)
N2^{ii}—Ta1—N3^{viii}	140.9 (11)	N3^{xiii}—Ta2—N3^{xiv}	135.8 (13)
N2^{iii}—Ta1—N3^{viii}	80.3 (12)	N3^{xiii}—Ta2—N3^{vi}	69 (2)
N2^{iv}—Ta1—N3^{v}	80.3 (12)	N3^{xiii}—Ta2—N3^{xii}	93.8 (18)
N2^{ii}—Ta1—N3^{v}	119.8 (14)	N4—Ta2—Ta1^{ix}	43.77 (17)
N2^{iv}—Ta1—N3^{vii}	140.9 (11)	N4^{x}—Ta2—Ta1^{x}	43.77 (16)
N2—Ta1—N3^{v}	140.9 (11)	N4—Ta2—Ta1	43.77 (16)
N2^{iii}—Ta1—N3^{v}	63.4 (10)	N4—Ta2—Ta1^{x}	105.8 (4)
N2—Ta1—N3^{vii}	80.3 (12)	N4^{x}—Ta2—Ta1	105.8 (4)
N2—Ta1—N3^{vi}	63.4 (10)	N4^{x}—Ta2—Ta1^{ix}	105.8 (4)
N2^{iv}—Ta1—N3^{viii}	63.4 (10)	N4—Ta2—Ta2^{xi}	63.1 (6)
N2^{iii}—Ta1—N3^{vi}	140.9 (11)	N4^{x}—Ta2—Ta2^{xi}	63.1 (6)
N2—Ta1—N3^{viii}	119.8 (14)	N4^{x}—Ta2—N1^{xi}	69.7 (5)
N2^{iii}—Ta1—N3^{vii}	119.8 (14)	N4—Ta2—N1	69.7 (5)
N2^{iv}—Ta1—N3^{vi}	119.8 (14)	N4^{x}—Ta2—N1	69.7 (5)
N2^{ii}—Ta1—N3^{vii}	63.4 (10)	N4—Ta2—N1^{xi}	69.7 (5)
N2^{iv}—Ta1—N4	140.7 (13)	N4—Ta2—N3^{vi}	70.3 (11)
N2^{ii}—Ta1—N4	117.8 (10)	N4—Ta2—N3^{xii}	132.7 (10)
N2^{ii}—Ta1—N4^{ix}	140.7 (13)	N4—Ta2—N3^{xiv}	70.3 (11)
N2—Ta1—N4^{ix}	140.7 (13)	N4^{x}—Ta2—N3^{xii}	70.3 (11)
N2^{iv}—Ta1—N4^{ix}	117.8 (10)	N4—Ta2—N3^{xiii}	132.7 (10)
N2—Ta1—N4	117.8 (10)	N4^{x}—Ta2—N3^{xiv}	132.7 (10)
N2^{iii}—Ta1—N4	140.7 (13)	N4^{x}—Ta2—N3^{vi}	132.7 (10)
N2^{iii}—Ta1—N4^{ix}	117.8 (10)	N4^{x}—Ta2—N3^{xiii}	70.3 (11)
N3^{viii}—Ta1—N3^{vi}	138.7 (16)	N4^{x}—Ta2—N4	126.1 (12)
N3^{v}—Ta1—N3^{vi}	150.7 (11)	Ta1—N1—Ta1^{x}	131.9 (13)
N3^{v}—Ta1—N3^{vii}	138.7 (16)	Ta1—N1—Ta2^{xi}	105.2 (2)

N3^{v}—Ta1—N3^{viii}	29 (2)	Ta1^{x}—N1—Ta2^{xi}	105.2 (2)
N3^{vi}—Ta1—N3^{vii}	29 (2)	Ta1^{x}—N1—Ta2	105.2 (2)
N3^{viii}—Ta1—N3^{vii}	150.7 (11)	Ta1—N1—Ta2	105.2 (2)
N4—Ta1—N3^{vi}	58.3 (8)	Ta2^{xi}—N1—Ta2	100.0 (10)
N4^{ix}—Ta1—N3^{vii}	92.6 (8)	N2^{xv}—N2—Ta1	124.5 (14)
N4—Ta1—N3^{vii}	58.3 (8)	N2^{xv}—N2—N3	113 (3)
N4^{ix}—Ta1—N3^{viii}	58.3 (8)	N3—N2—Ta1	122 (4)
N4—Ta1—N3^{viii}	92.6 (8)	Ta2^{xiii}—N3—Ta1^{vii}	88.4 (8)
N4^{ix}—Ta1—N3^{v}	58.3 (8)	N2—N3—Ta1^{vii}	124.0 (19)
N4—Ta1—N3^{v}	92.6 (8)	N2—N3—Ta2^{xiii}	119 (3)
N4^{ix}—Ta1—N3^{vi}	92.6 (8)	N3^{ii}—N3—Ta1^{vii}	75.7 (10)
N4—Ta1—N4^{ix}	35.5 (11)	N3^{ii}—N3—Ta2^{xiii}	124.7 (11)
Ta1^{ix}—Ta2—Ta1^{x}	120.49 (4)	N3^{ii}—N3—N2	113 (3)
Ta1—Ta2—Ta1^{ix}	83.40 (4)	Ta1—N4—Ta1^{ix}	144.5 (11)
Ta1—Ta2—Ta1^{x}	67.81 (4)	Ta2—N4—Ta1^{ix}	97.94 (9)
Ta2^{xi}—Ta2—Ta1^{ix}	60.24 (2)	Ta2^{i}—N4—Ta1	97.94 (9)
Ta2^{xi}—Ta2—Ta1^{x}	60.24 (2)	Ta2^{i}—N4—Ta1^{ix}	97.94 (9)
Ta2^{xi}—Ta2—Ta1	60.24 (2)	Ta2—N4—Ta1	97.94 (9)
N1—Ta2—Ta1	36.12 (17)	Ta2^{i}—N4—Ta2	126.1 (12)
N1^{xi}—Ta2—Ta1^{ix}	36.12 (17)	N4^{ix}—N4—Ta1	72.3 (6)
N1^{xi}—Ta2—Ta1	92.7 (4)	N4^{ix}—N4—Ta1^{ix}	72.3 (6)
N1^{xi}—Ta2—Ta1^{x}	92.7 (4)	N4^{ix}—N4—Ta2^{i}	116.9 (6)
N1—Ta2—Ta1^{ix}	92.7 (4)	N4^{ix}—N4—Ta2	116.9 (6)
N1—Ta2—Ta1^{x}	36.12 (17)	N5^{iii}—N5—N5^{xvii}	90.004 (9)
N1—Ta2—Ta2^{xi}	40.0 (5)	N5^{xvii}—N5—N5^{xvi}	45 (4)
N1^{xi}—Ta2—Ta2^{xi}	40.0 (5)	N5^{iii}—N5—N5^{xvi}	45 (4)
Ta1—N2—N3—Ta1^{vii}	−80 (3)	N2^{xv}—N2—N3—Ta1^{vii}	92 (3)
Ta1—N2—N3—Ta2^{xiii}	170.3 (12)	N2^{xv}—N2—N3—Ta2^{xiii}	−18 (2)
Ta1—N2—N3—N3^{ii}	8 (2)	N2^{xv}—N2—N3—N3^{ii}	179.998 (9)

Symmetry codes: (i) *x*, *y*, *z*−1; (ii) *x*, *y*, −*z*; (iii) −*x*, *y*, −*z*; (iv) −*x*, *y*, *z*; (v) *x*−1/2, −*y*+1/2, −*z*; (vi) −*x*+1/2, −*y*+1/2, *z*; (vii) −*x*+1/2, −*y*+1/2, −*z*; (viii) *x*−1/2, −*y*+1/2, *z*; (ix) −*x*, −*y*, −*z*; (x) *x*, *y*, *z*+1; (xi) −*x*, −*y*, −*z*+1; (xii) −*x*+1/2, *y*−1/2, −*z*+1; (xiii) −*x*+1/2, −*y*+1/2, −*z*+1; (xiv) −*x*+1/2, *y*−1/2, *z*; (xv) *x*, *y*, −*z*+1; (xvi) −*x*, −*y*+1, −*z*; (xvii) *x*, −*y*+1, *z*.